TÜBİTAK

Turk J Phys
36 (2012) , 343 – 351.

doi:10.3906/fiz-1107-3

Neutron cross-sections for ^{55}Mn in the energy range from 0.2 to 22 MeV

Abul Khaer Mohammad Rezaur RAHMAN
Department of Physics, Chittagong University, Chittagong 4331, BANGLADESH
e-mail: rezaur1970@yahoo.com

Received: 04.07.2011

Abstract

Neutron total and differential elastic scattering cross-sections for ^{55}Mn nucleus was calculated from different global spherical optical potential (SOP) sets for different neutron energies ranging from 0.2 MeV to 22 MeV using the well known computer program SCAT-2 on an IBM PC-AT. In addition, the angular distributions of elastically scattered neutrons at different neutron energies were calculated. The results were compared with those of the experimental data obtained from the EXFOR data file of NEA data bank. The best-fit potential parameter was thereby selected. It was observed that the best fit to the experimental values of the total cross-sections are obtained by SOP parameters of Kawai for ^{55}Mn. Furthermore, the variations of the total cross-sections as a function of real potential depth V_0 and real radius parameter r_0 were calculated to observe the sensitivity of these parameters towards the cross-sections.

Key Words: Optical model potential, SOP parameter, nuclear interaction cross section, angular distribution

1. Introduction

The interactions of nucleons with nuclei can be interpreted via different theoretical models. But no individual model or formula can explain the nuclear interaction cross-sections for the entire energy range. However, the average total neutron cross-sections can be interpreted by using the optical model, first proposed by Bethe [1] and then modified by many investigators [2–5]. They have shown that the total and elastic scattering cross-sections can be well fitted by the optical model potential with suitably adjusted parameters. The optical model provides the basis for many theoretical analyzes and/or evaluations of nuclear cross sections that are used in providing nuclear data for applied purposes. As well as offering a convenient means for the calculation of reaction, shape elastic and (neutron) total cross sections, optical model potentials are widely used in quantum-mechanical pre-equilibrium and direct-reaction theory calculations, and (most importantly) in supplying particle transmission coefficients for Hauser-Feshbach statistical-theory as used in nuclear data evaluations [6] Optical potentials are widely used in the Distorted-Wave-Born-Approximation (DWBA) analysis

[7]. A simultaneous analysis of elastic scattering, fusion, and total reaction cross sections can be performed by optical model calculations [8].

The most important task is to determine the optical model parameters [9, 10]. A lot of empirical information exists on its parameterizations [11]. Some investigations have been devoted to its energy dependence [12–15]. A very well established procedure is derivation of the optical model from a realistic nucleon-nucleon interaction using Brueckner theory [16–18]. There are two approaches to optical model: the microscopic approach and the phenomenological approach. Among these two approaches, the optical model has long been known to provide an excellent phenomenological description of nucleon-nucleus elastic scattering [19–25] for medium and heavy mass nuclei.

The present work contains a study of neutrons interactions with ^{55}Mn in the energy range 0.2 MeV to 22 MeV. Hence a phenomenological approach is deployed. The neutron total cross-section σ_t, shape elastic scattering cross-section σ_{sc}, compound nucleus cross-section σ_c for ^{55}Mn were calculated for different SOP sets. Then the total cross-sections σ_t were compared with the experimental data obtained from references [26–28, 29]. The angular distributions of ^{55}Mn for different energies were calculated and are compared with the experimental data supplied by IAEA. Variations of σ_t and σ_c as a function of real potential depth V_0, real radius r_R were also calculated to observe sensitivity of the parameters.

2. Optical model potential

O. Bersillon [2] used the general form of the optical potential as:

$U(r) = V_c(r) - V_r f(r, R_R, a_R) - i[\,-4\ W_s g(r, R_I, a_I) + W_v f(r, R_I', a_I')]$

$+\ C_{so} V_{so} h(r, R_{so}, a_{so})(\vec{l} \cdot \vec{S})$ (1)

The terms, from left to right, represent the Coulomb potential, the real volume potential, imaginary surface potential, imaginary volume potential and real spin orbit potential, respectively. This form of the optical potential is used in SCAT-2 [FORTRAN] computer program in our research works.

Also, above, $f(r, R_x, a_x) = [1 + \exp((r - R_x)/a_x)]^{-1}$ is the Woods-Saxon form factor. "x" denotes the real (x = "R") and imaginary (x = "I″) components. The relation $g(r, R_I, a_I)$=exp$[(r - R_I)/(a_I)][1 + \exp((r - R_I)/a_I]^{-2}$ is the derivative Woods-Saxon form factor with $R_I = r_I A^{1/3}$. And, the parameter $h(r, R_{so}, a_{so}) = 1/r\,(\mathrm{d}/\mathrm{d}r) f(r, R_{so}, a_{so}) = (1/r a_{so})\ \exp[(r - R_{so})/a_{so}][1 + \exp((r - R_{so})/a_{so})]^{-2}$ is the Thomas form factor with $R_{so} = r_{so} A^{1/3}$.

In our present calculations eight sets of parameters have been used. A discussion on each of them is found below. These global spherical optical parameterizations are presented in Table 1. The numerical values of the parameters of the optical potential can be obtained approximately by elementary arguments. Since the potential is the extension to positive energies of the potential of the simple shell model, its depth can be calculated from the Fermi gas model, using the relation between the depth and the radius. The depth of the imaginary part of the potential can be estimated from semi-classical arguments. The knowledge of the nuclear matter distribution gives $r = 1.2$ fm and $a = 0.65$ fm. Finally, the spin-orbit splitting is $V_{so} \approx 8$ MeV.

To determine the best fit parameters of the potential to a particular set of experimental data, it is usual to start with parameters known from previous analysis to be approximately correct, then to vary them to optimize the fit. It is thus usual in optical model analysis to keep the form factor parameters fixed to standard values and to vary only the potential depths. In this research work we use best-fit sets of parameters from previous

Table 1. Global spherical optical parameterizations. V_R = Real potential, W_D = Imaginary surface potential, W_v = Imaginary volume potential, V_{so} = Spin orbit potential, r = Radius parameter, a = Surface diffuseness parameter, and $\eta = \frac{N-Z}{A}$.

Parameter set	Potential		Radius parameter, r_i	a_i (fermion)
Set 2, Wilmore, Hodgson, 1964, $E \leq 15$MeV; A>40	$V_R = 47.01 - 0.2657E - 0.0018E^2$ $W_D = 9.52 - 0.53E$ $V_{so} = 7.0$		$1.322 - 7.6 \times 10^{-4}A + 4 \times 10^{-6}A^2 - 8 \times 10^{-9}A^3$ $1.266 - 3.7 \times 10^{-4}A + 2 \times 10^{-6}A^2 - 4 \times 10^{-9}A^3$ $1.322 - 7.6 \times 10^{-4}A + 4 \times 10^{-6}A^2 - 8 \times 10^{-9}A^3$	0.66 0.48 0.66
Set 4, Becchetti, Greenlees, 1969 E<50 MeV; A>40	$V_R = 56.3 - 0.32E - 24\,\eta$ $W_D = 13.0 - 0.25E - 12\,\eta$ $W_v = 0.22E - 1.56$ $V_{so} = 6.2$		1.17 1.26 1.26 1.01	0.75 0.58 0.58 0.75
Set 7, Madland, 1978, Actinide E<10 MeV	$V_R = 71.0$ $W_D = 7 + 0.4E$ $V_{so} = 7$ $\beta = 0.85$		$1.182 + 1.93 \times 10^{-4}A$ 1.21 $1.182 + 1.93 \times 10^{-4}A$	0.65 0.47 0.65
Set 8, Rapaport, 1979 E = 7 – 26 MeV A = 40 - 208	$V_R = 54.19 - 0.33E - (22.7 - 0.19E)\,\eta$ $W_D = 4.28 + 0.4E - 12.8\,\eta$ $W_D = 14.0 - 0.39E - 10.4\,\eta$ $W_v = 0$ $W_v = -4.3 + 0.38E$ $V_{so} = 6.2$	$E \leq 15$ $E > 15$ $E \leq 15$ $E > 15$	1.195 1.295 1.295 1.295 1.295 1.01	0.663 0.59 0.59 0.59 0.59 0.75
Set 10, Fu. Ketrick *Fe*	$V_R = 49.747 - 0.429E - 0.0003E^2$ $W_D = 11.8 - 0.21E$ $V_{so} = 6.2$		1.287 1.345 1.12	0.56 0.47 0.47
Set 12, Bersillon et al. ^{209}Bi 10^{-5} eV < E < 20 MeV	$V_R = 45.45 - 0.22E$ $W_D = 2.28 + 0.47E$ $W_D = 6.9 - 0.45E$ $W_v = 0.08E$ $V_{so} = 5.5$	E < 10MeV E > 10MeV E > 10MeV	1.265 1.235 1.235 1.235 1.08	0.65 0.5 0.5 0.5 0.6
Set 13, Kawai Ti, V, Cr, Mn , Fe, Co, Cu	$V_R = 51.33 - 0.331E_n$ $W_D = 8.068 + 0.112E_n$ $V_{so} = 7.0$		1.24 1.4 1.24	0.541 0.4 0.541
Set 14, Zongdi SU	$V_R = 48.54 - 0.31E$ $W_D = 2.4 + 0.4E$ $W_v = 0$ $V_{so} = 6$		1.27 1.27 0 1.2	0.68 0.58 0 0.5

investigations for ^{55}Mn and select the best fitting parameters among them. The Wilmore-Hodgson's potential [22] was proposed, for it has successfully predicted neutron cross sections from 1 MeV to 15 MeV for medium and heavy nuclei. Bechetti and Greenless [30] used as a basis of the data on proton scattering; with 40 sets for differential scattering cross-sections, 28 polarizations, and 8 reaction cross sections. They consider 30 sets of elastic angular distributions, 4 polarizations and 28 total cross sections for neutron scattering. This is also mass dependent. Rapaport et al [31] based their results on fitting of neutron elastic angular distributions in the energy range from 7 MeV to 26 MeV for nearly closed-shell nuclei. The regional parameterization by Madland [32] is more suitable for low energies up to 3 MeV in the actinide series. The parameters of Bersillon (set 12) have been obtained from their works on neutron scattering of ^{209}Bi from beam energy 0.001 eV to 20 MeV. These five optical parameters sets are built into the SCAT-2 program. Parameter set 10 is due to Fu. Ketrick, and set 13 due to Kawai, are obtained from Global SOP Table; and set 14 is comes from Su. Zongdi [23] is from his works. Parameter sets 2, 4, 7, 8, 10, 12, 13 and 14 were used as inputs in the present calculations.

3. The Results and Analyses

3.1. Neutron total cross-sections σ_t from ^{55}Mn

The total cross-section σ_t for the interaction of neutrons with ^{55}Mn are calculated for eight global spherical optical potential (SOP) parameter sets 2, 4, 7, 8, 10, 12, 13, 14 (Table 1) at neutron energies 0.2, 0.5, 0.7, 1, 2, 3, 4, 5, 6, 7, 8, 10, 12, 14, 16, 18, 20 and 22 MeV. The predicted results were compared in each case with the experimental total cross-section σ_t data, and are shown in Figures 1 and 2.

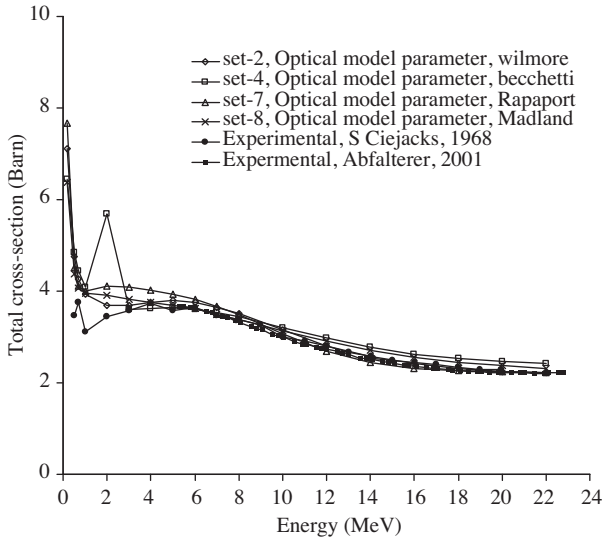

Figure 1. Neutron total cross-section for ^{55}Mn using parameter sets 2, 4, 7, 8.

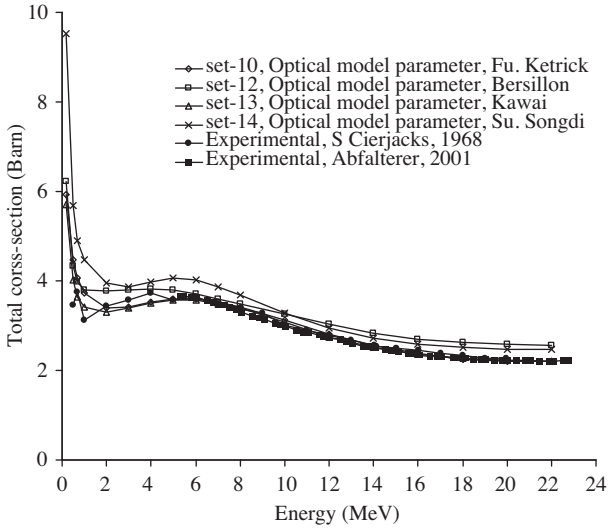

Figure 2. Neutron total cross-section for ^{55}Mn using parameter sets 10, 12, 13 and 14.

The experimental data from energies 0.5 MeV to 19.982 MeV are taken from the literature [26, 29]. From figures it is observed that the total neutron cross-section for ^{55}Mn has a valley at 1 MeV and a broad maximum from 3 to 10 MeV. The theoretical calculations for the sets 10, 13, 14 give the valley at around 1.5 MeV and the broad maxima at around 6 MeV. The calculated curve due to parameter set 12 (Bersillon) has no valley and broad maxima and has a turning from higher cross-section to lower at 1 MeV energy. The calculation due to parameter set 7 has a valley at 1 MeV. The calculated curve goes through the upper side of the experimental curve for $E_n < 9$ MeV and through the lower side of that for $E_n > 9$ MeV. The calculation is based on parameter set 2 and 4 have the valley at around 2 MeV and a broad maxima at around 6 to 7 MeV. It is observed that all the parameter set discussed about are not suitably agreed with the experimental data. Among all these, however, the calculated curve due to the set 13 (Kawai) gives the best agreement with the experimental value for all energies except the lower one up to 5 MeV. There are fluctuations in the experimental total cross-section of ^{55}Mn at lower energies because of resolved resonances in the cross-section.

3.2. Angular distribution of the shape of the ^{55}Mn elastic differential cross-section $d\sigma_{el}/d\Omega$

The phenomenological model fits to the individual data sets provided good representation of the data for set 13 due to Kawai in case of ^{55}Mn. The global phenomenology provides average fit as expected and does a

good job describing the energy dependence of the differential cross-section from energy 3.0 MeV to 11.01 MeV. The characteristic properties of differential cross-sections as a function of centre of mass angle have been studied. Parameter set 13 due to Kawai gives best agreement with the experimental total cross-sections data among all the predicted parameter sets. So, the angular distribution in the energy region 3.0 MeV to 11.01 MeV is studied, by using the parameter set 13 and the computer program SCAT-2 of O. Bersillon. The measurement made in the present investigation includes angular distribution in energies $E_n = 3$, 4, 6.09, 8.05 and 11.01 MeV, at center of mass angle from 0° to 180° at a step of 2.5° for neutron elastically scattered from ^{55}Mn [2].

Comparison between the calculated and the measured data for ^{55}Mn at 3 MeV for the neutron elastic scattering differential cross-sections are shown in Figure 3. The experimental data are taken from the literature [27, 28]. A single minimum is observed at 72.5°. The experimental data points agree with the theoretical data. The angular distribution pattern is poorly recovered. The results are almost same for the prediction due to 4 MeV neutron energy. The experimental data are also taken from the same literature. The graphical representation of the result is shown in Figure 4. Here a second minimum is observed at 155°. The results are also presented for neutron energy 6.09 MeV. The comparison between the theoretical and the experimental data is shown in Figure 5. The first and the second minima occurred at 65° and 140°. The experimental values do not agree with the minima and maxima of the predicted curve and the experimental values poorly recovered the pattern of the curve. Figure 6 shows the theoretical and experimental comparison of angular distribution for neutron scattering at energy 8.05 MeV. In the theoretical curve the first and the second minima occurred at 62.5° and 135°. The first and the second minima of the experimental curve occurred at 70° and 125° respectively. The experimental observations are taken from the literature [27, 28]. The graphical representation of the results for 11.01 MeV neutron scattered from ^{55}Mn are shown in Figure 7. The experimental angular distribution data are taken from the literature [33, 34]. Both of the theoretical and the experimental curves have two minima and three maxima, but the experimental values are distorted from theoretical values after 50°.

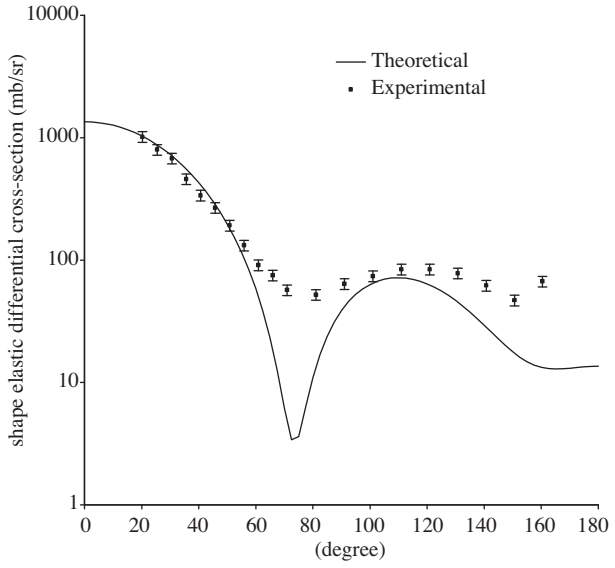

Figure 3. Angular distribution for the interaction of neutron with ^{55}Mn for 3.0 MeV neutron energy.

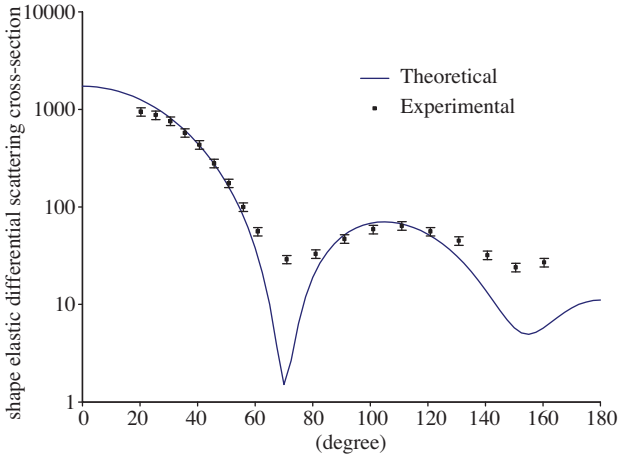

Figure 4. Angular distribution for the interaction of neutron with ^{55}Mn for 4.0 MeV neutron energy.

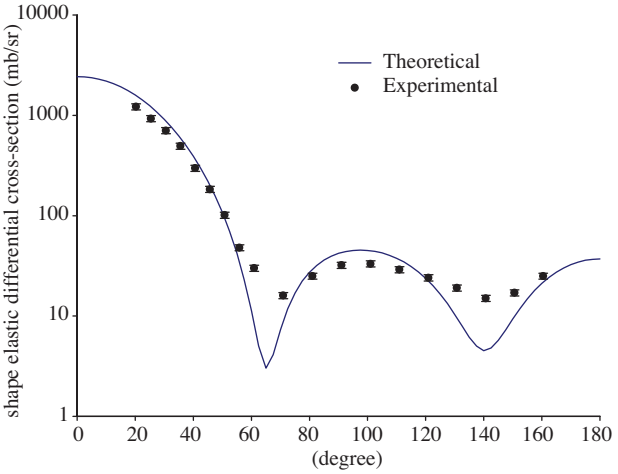

Figure 5. Angular distribution for the interaction of neutron with ^{55}Mn for 6.09 MeV neutron energy.

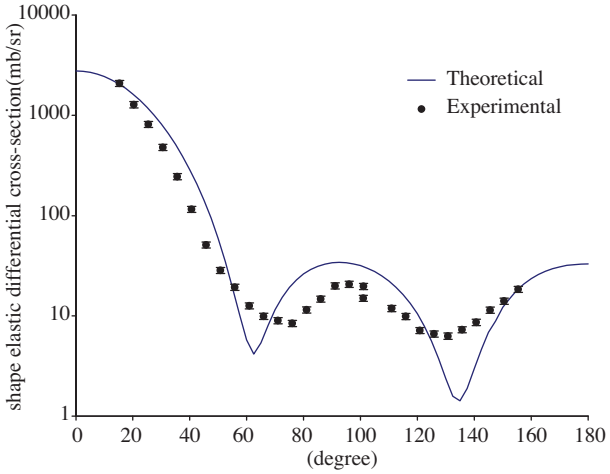

Figure 6. Angular distribution for the interaction of neutron with ^{55}Mn for 8.05 MeV neutron energy.

Finally, it can be concluded that the angular distribution for the neutron scattering from ^{55}Mn fit well at the lower centre of mass angle but in the higher angle the distributions give the disagreement. The minima and the maxima of theoretical curve are shifted from the experimental values for all neutron energies.

3.3. Variation of the cross-section of ^{55}Mn with parameters

The variation of the parameters in the optical model analysis is most important to understand the interaction of various particles with nuclei. The variation of the total and compound nuclear cross-section as the functions of the real potential depth and real radius parameters are studied in the interaction of neutron with ^{55}Mn for neutron energies, E_n = 0.5, 0.7, 1, 5, 10, 16, 22 MeV.

The variation of total cross-section σ_t as a function of real potential depth V_0 is shown in Figure 8. The results for the neutron energies 0.2 to 22 MeV, except 5 MeV, show almost linear increment. At energy 5 MeV, σ_t decreases.

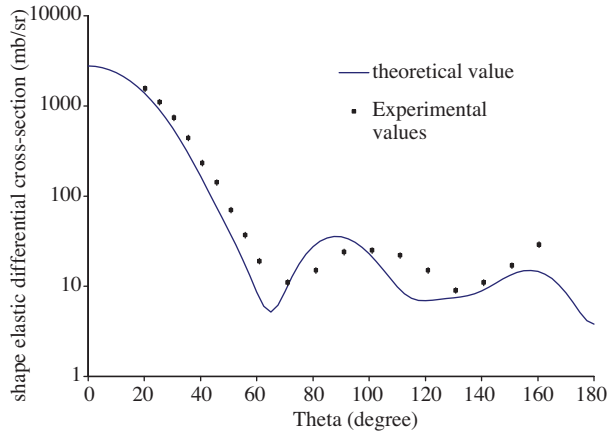

Figure 7. Angular distribution for the interaction of neutron with ^{55}Mn for 11.01 MeV neutron energy.

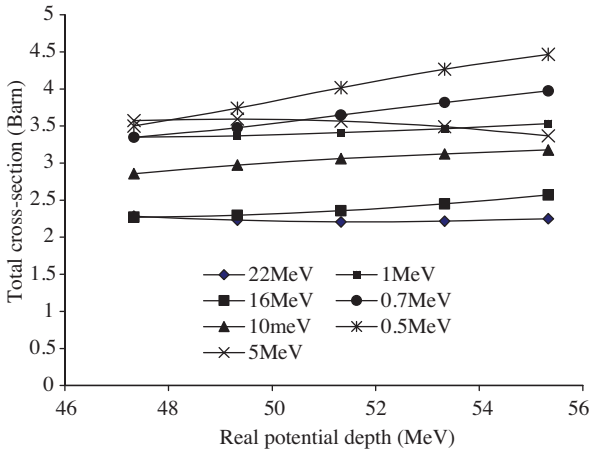

Figure 8. Variation of the total cross-section of ^{55}Mn with variation of the real potential depth $(V - V_0)$; SOP set 13 and its potential V_0 = 51.337 MeV, taken as central value.

Figure 9 shows the graphical results for the variation of σ_c as a function of V_0. For neutron energy of 0.5 MeV, σ_c was observed to fluctuate. Cross-section σ_c decreases linearly at 10 MeV neutron energies, but increases or remain almost constant for other energies.

The graphical representations of the variation of σ_t as a function of real radius parameter r_0 are shown in Figure 10. The total cross sections increase with the variation of real radius parameter; some with small increments, some with comparatively large increments.

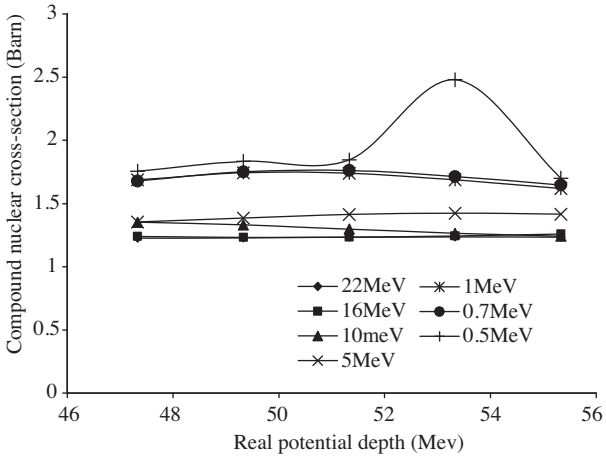

Figure 9. Variation of the compound nuclear cross-section of ^{55}Mn with variation of the real potential depth $(V - V_0)$; SOP set 13 and its potential $V_0 = 51.337$ MeV, taken as central value.

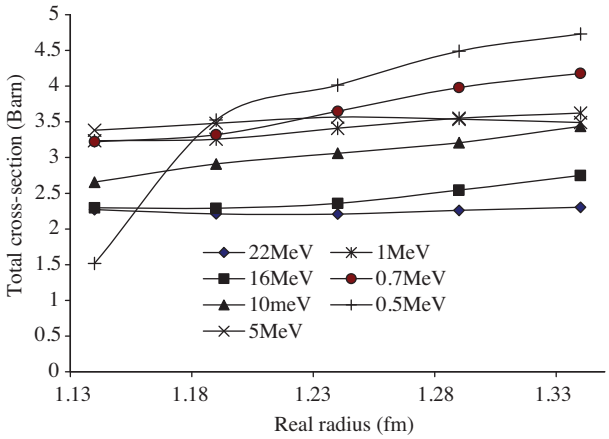

Figure 10. Variation of the total cross-section of ^{55}Mn with variation of the central radius $(r - r_0)$; SOP set 13 and its potential $r_0 = 1.24$ fm taken as central value.

Figure 11 shows the graphical representation of σ_c as a function of real radius parameter r_0. At low energies the compound nuclear cross-section decreases from the central value on both sides. For 10 MeV neutron σ_c decreases with the increment of r_0. Cross-section σ_c increases slowly for other predicted energies.

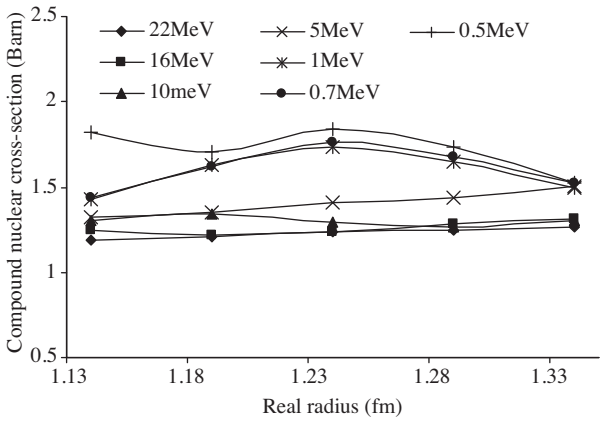

Figure 11. Variation of the compound nuclear cross-section of ^{55}Mn with variation of the central radius $(r - r_0)$; SOP set 13 and its potential $r_0 = 1.24$ fm taken as central value.

4. Conclusions

The following are the conclusions of the present study.

(a) The calculated total cross-sections for ^{55}Mn are in agreement with the measured available values above 2 MeV for almost all the sets of global spherical optical model parameters. However, the parameter set 13 due to Kawai shows the best agreement for the energy above 2 MeV. The experimental total neutron cross-sections have considerable fluctuations up to 2 MeV because of resolved resonances in the cross-sections.

(b) For a given neutron energy, the behavior of the angular distributions show an excellent agreement with the experimental values at forward angles but at the backward angles the agreement is found not so satisfactory. Also, the angular distribution patterns in minima are poorly reproduced.

(c) It is very difficult to get a unique set of parameters, which can accurately describe as much as experimental data as possible in the wide region of neutron energies and nuclear masses. No parameterization as mentioned previously can reproduce the experimental data of lower energies and higher energies at the same time.

(d) The real potential depth V_0 and the real radius parameters r_0 are the most responsive parameters in the SOP. Small changes in V_0 and r_0 lead to great variations in the cross-sections. For energies below 1 MeV, the total cross-sections with increasing V_0 or r_0 fluctuate largely. However, for the higher neutron energies, the variations of total cross-section with increasing SOP parameter are small.

The results also show that the variations of the cross-section with increasing the SOP parameters are very different for different energies. The total cross-sections increase with some SOP parameter for some energies, decrease for some energies and fluctuate or do not change for other energies.

However, the SOP parameters set 13 for ^{55}Mn can be used for the calculation of total cross-sections, angular distributions etc. among the eight parameter sets under study for reasonable agreement with the experimental results.

Acknowledgement

The author is indebted to *Professor Md. Nurul Islam*, Dean, Faculty of Science, Northern University of Bangladesh for his keen supervision and suggestion about this research work.

References

[1] H. Bethe, *Phys. Rev.*, **57**, (1940), 1125.

[2] O. Bersillon, Lectures on the computer code SCAT-2, Workshop on Applied Nuclear Theory and Nuclear Model Calculations for Nuclear Technology Applications, (Trieste. 1988).

[3] H. H. Berschall, *Phys. Rev.*, **86**, (1952), 431.

[4] H. Feshbach, C. E. Porter and V. F. Weisskopf, *Phys. Rev.*, **96**, (1954), 448.

[5] R. D. Woods and D. C. Saxon, *Phys. Rev.*, **95**, (1954), 577.

[6] International Atomic Energy Agency, Handbook for Calculations of Nuclear Reaction Data, Vienna, RIPL-2 IAEA, IAEA-Tecdoc-**1506**, (2006), 47.

[7] B. V. Carlson, Optical model Calculations with the code ECIS95, Lectures given at the workshop on Nuclear data and nuclear reactors: Physics, design and safety, Treasty, (13March - 14April 2000).

[8] A. Gómez Camacho, P. R. S. Gomes, J. Lubian, *Phys. Rev. C*, **82**, (2010), id. 067601.

[9] Satoshi Kunieda, Nobuhiro Shigyo and Kenji Ishibashi, *Journal of Nuclear Science and Technology*, **41,** (2004), 1047.

[10] Mehmet Ertan Kürkçüoğlu, Hüseyin Aytekin, İsmail Boztosun, *G.U.J. Sci.*, **19,** (2006), 105.

[11] G. M. Perey and F. G. Perey, *At. Data and Nucl Data tables*, **17**, (1976) 1.

[12] P. A. Moldauer, *Nucl. Phys.*, **47,** (1963), 65.

[13] C. Mahaux and R. Sartor, *Nucl. Phys.* A, **484**, (1988), 205.

[14] C. Mahaux and R. Sartor, *Nucl. Phys. A*, **480**, (1988), 381.

[15] C. H. Johnson and C. Mahaux, *Phys. Rev. C,* **25**, (1988), 85.

[16] H. Feshbach, D. C. Peaslee and V. F. Weisskopf, *Phys. Rev.,* **71**, (1947), 145.

[17] H. Feshbach, V. F. Weisskopf, *Phys. Rev.,* **76**, (1949), 1550.

[18] J. H. Dave and C. R. Gould, *Phys. Rev. C,* **28**, (1983), 2212.

[19] M. Jamin and C. Mahaux, *Phys. Rev. C,* **34**, (1986), 2084.

[20] N. Olsson et al., *Nucl. Phys. A,* **513**, (1990), 228.

[21] J. Rapaport, *Phys. Rev.,* **87**, (1982), 25.

[22] D. Wilmore and Hodgson, *J. Phys. G,* **11,** (1985), 1007.

[23] Su-Zungdi, *INDC (CRP)*-**013/LI INT1,** (1988), 1.

[24] K. Yabana et al., *Phys. Rev. C,* **45**, (1992), 2909.

[25] M. N. Islam et al., *J. Phys. G.,* **20**, (1994), 1471.

[26] S. Cierjacks, P. Forti, D. Kopsch, L. Kropp, H. Unseld. J. Nebe, *KFK,* **1000,** (1968), Suppl. II.

[27] B. Holmquist, T. Wiedling, *Sweden AE* - **366,** (1969), 85.

[28] B. Holmqvist, T. Wiedling, S.G. Johansson, G**.** Lodin, A. Kiss, B**.** Gustavsson and B. Antalkovic, *Nucl. Phys.* A, **146,** (1970), 321.

[29] W. P. Abfalterer, F. B. Bateman, F. S. Dietrich, R. W. Finlay, R. C. Haight, G. L. Morgan, *Phys. Rev. C,* **63**, (2001) 044608. (Data retrieve from the EXFOR database version of October 3, 2011)

[30] F. D. Beccehetti and G. W. Greenless, *Phys. Rev.,* **182**, (1969), 1190.

[31] J. Rapaport, V. Kul Karni and R. N. Finlay, *Nucl. Phys.*, **1330**, (1979), 15.

[32] D. C. Madland and P. G. Young, Conf. on neutron Physics and nucl. data for reaction and other application, Harwell OECK, (1978), 349.

[33] J. C. Ferrer, J. D. Carlson, J. Rapaport, *Nucl. Phys. A*, **275,** (1977), 325.

[34] J. C. Ferrer, J. D. Carlson and J. Rapaport, *Phys. Lett. B,* **62,** (1976), 399.